encit 2020

ABCM Associação Brasileira de Engenharia e Ciências Mecânicas

18th Brazilian Congress of Thermal Sciences and Engineering
November 16–20, 2020 (Online)

ENC-2020-0706
ANALYSIS OF OPEN-SOURCE CODE CAPACITY TO SOLVE TRANSONIC FLOW PROBLEMS

Henrique Matos Campos
Aluisio Viais Pantaleão
Faculdade de Engenharia de Ilha Solteira, Ilha Solteira, São Paulo, 15385-000, Brazil
hmatoscampos@gmail.com,aluisio.pantaleao@unesp.br

Abstract. *Nowadays, the CFD predicts with accuracy many aerodynamics phenomena, and the results of this numerical analysis are used in aircraft projects and operation to generate gains. However, the transonic flow regime still a challenge for engineering, since in literature are found few solutions in this regime, and most of them using proprietary codes. So our question is: are the open-source CFD codes currently existing capable of solving transonic flows? To answer this question was analyzed the capability of SU2 to simulate the transonic flow over an ONERA M6 wing. In this study was developed a numerical methodology testing different turbulence models and ensuring the grid convergence. After that, the results evaluated were compared with experimental data provided by the literature for various test conditions.*

Keywords: *CFD, Open-source, SU2, Transonic Flow, ONERA M6.*

1. INTRODUCTION

Nowadays, Computational Fluid Dynamics (CFD) plays a crucial role in the aeronautical industry for the project and operation of aircraft. Due to CFD, it is possible to prevent catastrophic aeroelastic instabilities, predict aeroelastic deformations, and the effects of flexibility in structural mechanics in flight. So, this kind of analysis allows design aircraft with safer, lighter, and more efficient structures, reducing costs in production and ensuring better use in operation.

However, the benefits of CFD depends on the accuracy of the results obtained by the methodology, being the transonic regime one case for this analysis.

Usually, the analyses of the transonic regime are complex and inaccurate. What happens due to this regime keeps characteristics of subsonic and supersonic flows.

To keep the state of the art of CFD for aeroelastic prediction, an initiative of researchers linked to the AIAA (American Institute of Aeronautics and Astronautics) led by NASA developed in 2012 the Aeroelastic Prediction Workshop (AePW), more details are presenting in AePW-1 (2015).

In its second edition, the AePW-2 (more information about are providing in AePW-2 (2016)) discussed the transonic flow over the Benchmark Supercritical Wing (BSCW). Since the transonic flow until nowadays still a difficult problem for CFD analysis, the goal of the workshop was to see which groups were capable of solving this problem with reasonable accuracy.

All the test cases proposed by AePW-2 were solved by two groups around the world, one from Embraer; and other from the union of the Israeli CFD Center and Israel Institute of Technology.

The Embraer group, as presented in Begnini *et al.* (2016), used CFD++ and CMSoft Aero (ATS (2020) provides more details about CFD++ and CMSoft (2020) more about CMSoft Aero) for the analysis; and The Israeli CFD Center group, as seen in Raveh *et al.* (2018), used EZNSS for the solution, being EZNSS an in-house multizone Euler/Navier-Stokes flow solver.

As we can see, all the solutions for AePW-2 used proprietary software or in-house codes for the analyses. However, due to licensing costs and difficulties and required time of software implementation, the use of these kinds of software is restricted to academia, where open-source codes are a better option.

In this context, SU2 and OpenFOAM are CFD open-source codes used for various users worldwide, with industrial and scientific applications to evaluate computational fluid dynamics, heat transfer, fluid-structure interaction, multiphase flow, and aerodynamics. Both software receives constant updates and upgrades from the community; and also grant the user the possibility of making his on implementations what can be attractive for academia.

So, our question during the study was: are the open-source CFD codes available capable of solving transonic flows?

To answer this question was decided to use SU2, an open-source CFD code created by SU2 Foundation, more detail about this software is providing in SU2 Foundation (2020).

SU2 was used in the research due to the software been developed for aeronautic applications, as presented in SU2Foundation (2020). Also, the software has already been tested for transonic flow cases, as found in Sanchez *et al.* (2016).

Being BSCW a very complex wing geometry, it was decided to simplify our study adopting a simpler geometry model, in this case choosing the ONERA M6 wing, this choice was due to the fact of this wing be a classic validation case for transonic flow applications.

What leads us to the objective of this study: test SU2 capability to solve the transonic flow problem over the ONERA M6 wing geometry.

This study is import because: gives user's information about the capability of the open-source software to solve the transonic flow problem; stimulate the use of open-source codes in academia and help the code development and validation. Also, the knowledge and improvement of CFD techniques are paramount within the scenario of the technological development of the Brazilian aeronautical industry.

2. THEORETICAL BACKGROUND

2.1 Governing equations of fluid flow

The CFD methodology consists of the solution of the governing equations of fluid flow using numerical methods. For the current study, our interest was to use CFD to solve the equations of mass, momentum, and energy conservation for a compressible, transonic, turbulent, and steady-state Newtonian and isotropic fluid flow.

According to the hypotheses considered, the fluid flow can be determined by equations 1, 2 and 3.

$$\nabla \cdot [\rho \vec{v}] = 0 \tag{1}$$

$$\nabla \cdot [\rho \vec{v}\vec{v}] = \nabla \cdot [\mu \nabla \vec{v}] - \nabla p + S_M \tag{2}$$

$$\nabla \cdot [\rho c_p \vec{v} T] = \nabla \cdot [k \nabla T] + S_T \tag{3}$$

Where: ρ is the density of the fluid, $\vec{v}$ is the velocity vector, μ is the fluid dynamic viscosity, p is the pressure, S_M is the source term of momentum, Cp is the specific heat at constant pressure, T is the temperature, k is the thermal conductivity, and S_T is the source term of energy.

As the modeled fluid flow is compressible, so was needed an equation of state to close our system of equations and verify the relation between density, pressure, and temperature.

As all the test cases analyzed during the study uses R-134a as fluid, approaching this as an ideal gas. Considering this hypothesis was decided to use Sutherland's law. Equation 4 gives the correlation presented by Sutherland's law.

$$\mu = \mu_{ref} \left(\frac{T}{T_{ref}} \right)^{3/2} \frac{T_{ref} + S}{T + S} \tag{4}$$

In Equation 4: T_{ref} is a reference temperature, μ_{ref} is the dynamic viscosity at the reference temperature and S is the Sutherland temperature.

2.2 Turbulence models

Since the fluid flow is considered turbulent, was used the Reynolds-averaged Navier-Stokes equations (RANS) to compute the turbulence.

Based on the Reynolds decomposition of the properties, the governing equations (presented in 1, 2, and 3) results in a closure problem, according Moukalled *et al.* (2016). To solve this problem was needed to resort to a turbulence model to complete the resulting system of equations.

For the study, were selected two turbulence models, the Spalart-Allmaras Turbulence Model (SA) and the Menter Shear Stress Transport Turbulence Model (k-ω SST). The choice of these turbulence models was due to both had being developed for aerospace applications.

Both turbulence models selected supposes an $y+ = 1$ and assumes the Boussinesq assumption in their formulation.

The Boussinesq assumption consists of am approach to computing the Reynolds stress Tensor, being its mathematical formulation presented in equation 5.

$$\tau^R = -\rho \overline{\vec{v}\vec{v}} = \mu_t \{\nabla \vec{v} + (\nabla \vec{v})^T\} - \frac{2}{3}\{\rho k + \mu_T (\nabla \cdot \vec{v})\}[I] \tag{5}$$

In Equation 5 τ^R is the Reynolds stress Tensor, μ_T is the turbulent dynamic viscosity, and $[I]$ is the identity matrix.

According to Rumsey (2018), the SA turbulence model is a one-equation turbulence model that solves Equation 6 to evaluate the kinematic eddy turbulent viscosity (ν_T).

$$\frac{\partial \tilde{\nu}}{\partial t} + (\nabla \cdot \vec{v}) \nabla \tilde{\nu} = c_{b1}(1 - f_{t2}) \tilde{S} \tilde{\nu} - \left[c_{w1} f_w - \frac{c_{b1}}{\kappa^2} f_{t2} \right] \left(\frac{\tilde{\nu}}{d} \right)^2 + \frac{1}{\sigma} \{\nabla \cdot [(\nu + \tilde{\nu}) \nabla \tilde{\nu}] + c_{b2} \nabla \tilde{\nu} \nabla \tilde{\nu}\} \tag{6}$$

Being in Equation 6: ν the kinematic viscosity ($\nu = \mu/\rho$).

Rumsey (2018) also presents more detail about the SA turbulence model, being in this, exposed the complete formulation, the constants, and the boundary condition required.

As presented in Rumsey (2020), the k-ω SST turbulence model is a two-equation turbulence model that solves Equation 7 for the turbulence kinetic energy (k) and Equation 8 for the specific rate of dissipation of the turbulence kinetic energy k into internal thermal energy (ω).

$$\frac{\partial(\rho k)}{\partial t} + \nabla \cdot (\rho \vec{v} k) = P - \beta^* \rho \omega k + \nabla \cdot [(\mu + \sigma_k \mu_t) \nabla k] \tag{7}$$

$$\frac{\partial(\rho \omega)}{\partial t} + \nabla \cdot (\rho \vec{v} \omega) = \frac{\gamma}{\nu_t} P - \beta \rho \omega^2 + \nabla \cdot [(\mu + \sigma_\omega \mu_t) \nabla \omega] + 2(1 - F_1) \frac{\rho \sigma_{\omega 2}}{\omega} \nabla k \nabla \omega \tag{8}$$

Rumsey (2020) presents more detail of the formulation, the constants, and boundary conditions required for the k-ω SST turbulence model.

3. METHODOLOGY

3.1 Analyzed geometry

In the study, was used the ONERA M6 wing geometry. The geometry characteristics of this wing, according Slater (2015), are presented in Table 1.

Table 1: ONERA wing characteristics according Slater (2015).

Span (b)	1,1963 m
Mean Aerodynamic Chord (c)	0,64607 m
Aspect Ratio	3,8
Taper Ratio	0,562
Leading-edge Sweep	30,0°
Trailing-edge Sweep	15,8°

Typically ONERA M6 is divided into six sections for analysis, as presented in Figure 1. The experimental data available for this geometry is the pressure coefficient measured along the upper and the lower surface of each section, following the experiment of Schimitt and Charpin (1979). According to Slater (2015) the accuracy of the measurements at Mach 0,84 was of +/- 0.02. It was evaluated, during the study, the pressure coefficient (Cp) in sections 2 and 3 (presented in figure 1) of the wing.

3.2 Flow conditions

The study was divided into two parts for a better result discussion. However, both parts took the same assumptions for fluid flow modeling of the governing equations. As presented during Section 2.was considered that:

- **The flow is**: compressible, transonic, turbulent, and steady-state.
- **The fluid is**: Newtonian and isotropic.

For the study, was considered three test cases found in Schimitt and Charpin (1979) for the ONERA M6 wing. The flow conditions analyzed in each test case are present in Table 2.

Table 2: Flow conditions for the studied cases of Schimitt and Charpin (1979).

Case	**2306**	**2308**	**2309**
Mach (Ma)	0,8398	0,8395	0,6998
Reynolds Number (Re)	$11{,}71 \cdot 10^6$	$11{,}72 \cdot 10^6$	$11{,}74 \cdot 10^6$
Angle-of-Attack (AoA)	1,07°	3,06°	0,04°
Angle-of-Sideslip (AoS)	0,00°	0,00°	0,00°

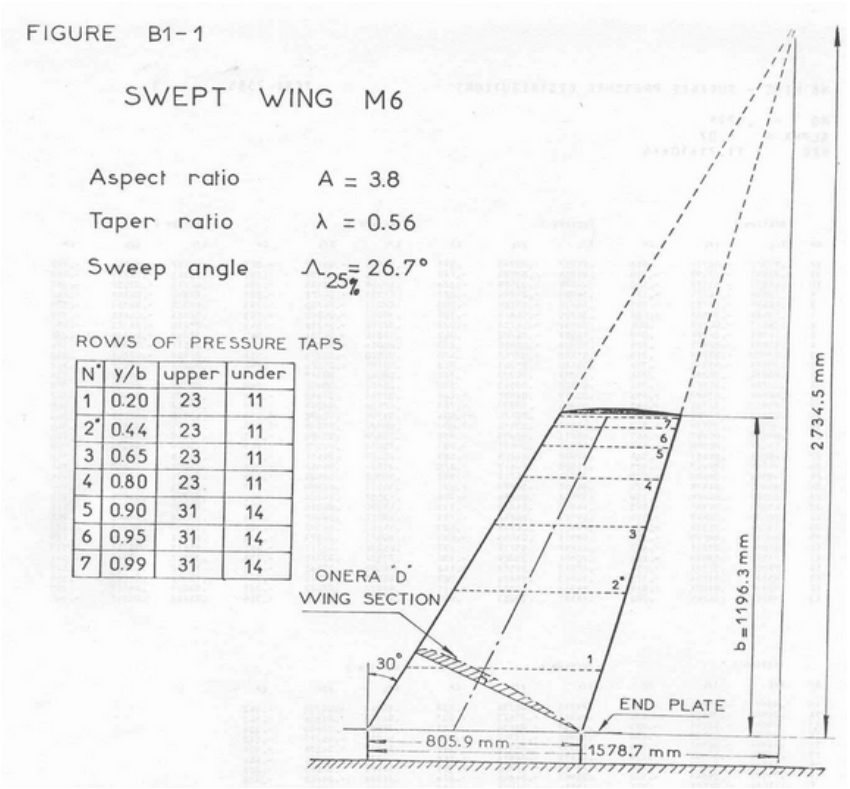

Figure 1: Layout of the ONERA M6 wing according Slater (2015).

3.3 Softwares

For all the computational analyses, was used the SU2 version v6.2.0 Falcon.

As SU2 native mesh format is the .su2 and since just a few mesh generators like Pointwise and Gmsh can generate .su2 meshes, it was decided to use .cgns mesh format to generate the meshes, in this case, was used Ansys Mesh of Ansys 2020 academic license for the grid generation, more details in Ansys (2020).

For the post-processes, was used Paraview 5.7.0.

3.4 Numerical Methods

As presented during Section 2.was used Sutherland's law as the viscosity model and Constant Prandtl as the conductivity model. To compute the gradient was used the Green-Gauss gradient scheme. The Flexible Generalized Minimal Residual method (FGMRES) method adopting ILU as a preconditioner, was used as a solver for the linear system of equations. For the flow numerical method definition, the Jameson-Schmidt-Turkel (JST) scheme adopting Venkatakrishnan as a slope limiter, was used for the convective numerical method. And for the turbulent numerical method definition was used Scalar Upwind as a convective numerical method adopting Venkatakrishnan as a slope limiter.

Besides that, the numerical methodology developed only used turbulence models. For this analysis, the study didn't make use of any wall function.

3.5 Simulation of the case 2308 and mesh generation

In the first part of the study, was simulate the flow condition presented in Slater (2015), the case 2308 of Schimitt and Charpin (1979). For this part, was used benchmarking meshes provided into the SU2 tutorials, found in Economon (2014b), and generated our meshes.

For this part, Grid Convergence Index (GCI) analysis was done, following the procedure proposed by Celik *et al.* (2008) to guarantee the convergence of the meshes developed by the authors.

For all the generated meshes, the ONERA M6 wing was centered in a semispherical farfield of radius equivalent of 20 chords, as can be seen in figure 2. The figure also presents the boundary conditions adopted in the analysis.

For the mesh generation, an $y+ = 1$ was adopted, following the requirement of the Spalart-Allmaras and k-ω SST turbulence models. Table 3 presents more detail about the generated meshes.

During the first part of the study, was analyzed the accuracy of the results obtained by the turbulence models adopted to select the one that provided better results, also including the results obtained by the simulation of the case using Euler

equations besides of Navier-Stokes equations.

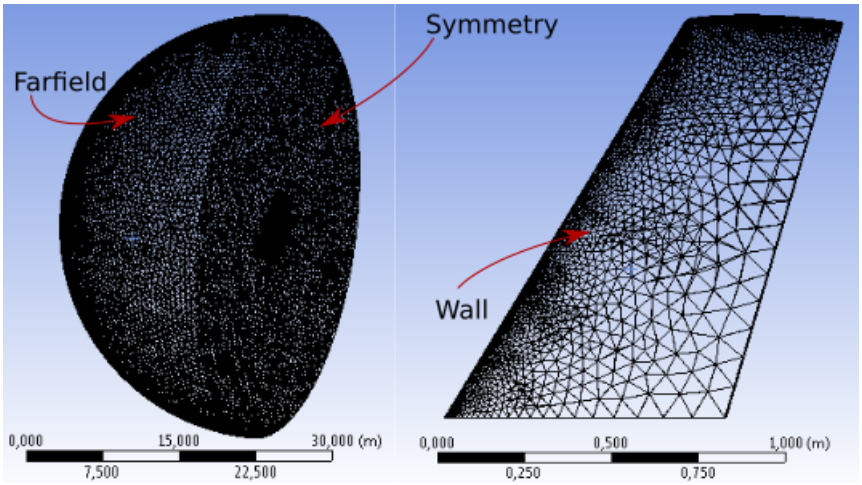

Figure 2: Layout of the ONERA M6 wing according Slater (2015).

Table 3: Used mesh information.

Mesh	**Navier-Stokes benchmarking mesh**	**Euler benchmarking mesh**	**Coarse mesh**	**Intermediary mesh**	**Fine mesh**
Number of elements	$4,3 \cdot 10^4$	$5,8 \cdot 10^5$	$2,11 \cdot 10^5$	$8,99 \cdot 10^5$	$1,99 \cdot 10^6$
y+	-	-	1	1	1
Number of layers	-	-	38	38	38
Aspect Ratio	-	-	1.2	1.2	1.2
First element height (m)	-	-	$1.654 \cdot 10^{-6}$	$1.654 \cdot 10^{-6}$	$1.654 \cdot 10^{-6}$

3.6 Simulation of the case 2306 and 2309

In the second part of the study, was verified how generalist was the methodology developed by comparing the results obtained by the simulation of the finest mesh done by the authors with the literature data provided by Schimitt and Charpin (1979) for other test cases. For this stage of the study, were selected the test cases 2306 and 2309 proposed by Schimitt and Charpin (1979).

4. RESULTS

4.1 Case 2308 analysis

For the case 2308, were plotted 41 points for the coarse mesh, 88 points for the intermediary mesh, and 108 points for fine mesh developed by the authors, and 88 points for the Benchmarking mesh provided in Economon (2014b), comparing these with the 35 points provided by the experimental data found in Slater (2015), for sections 2 and 3.

Figure 3 presents the results obtained from the numerical analysis of case 2308 using the SA turbulence model, following the procedure proposed by Economon (2014b). As seen in the Figure, for the case 2308, the results obtained along the lower surface of the wing sections almost fit with the experimental data and the benchmarking mesh results. For the upper surface, however, the coarse mesh isn't capable of capturing the behavior found in experimental data for the case. But the fine and the intermediary meshes were capable of fit with reasonable accuracy with the experimental data.

As can be seen, the discontinuity presented around 0,4-0,6 of x/c isn't captured with precision by the meshes developed by the authors or the benchmarking mesh.

Another issue found during the analysis was the capture of the results in the trailing edge, where, due to the geometry characteristics, were impossible to generate elements with good quality, leading the numerical results to diverge from the experimental data in this region, this is clear in the coarse mesh curves but still sustained in the intermediary and the fine mesh.

Then, following the procedure of Celik *et al.* (2008), was perform the GCI analysis for the case 2308 to secure the convergence of the mesh. The results found are presented in Table 4.

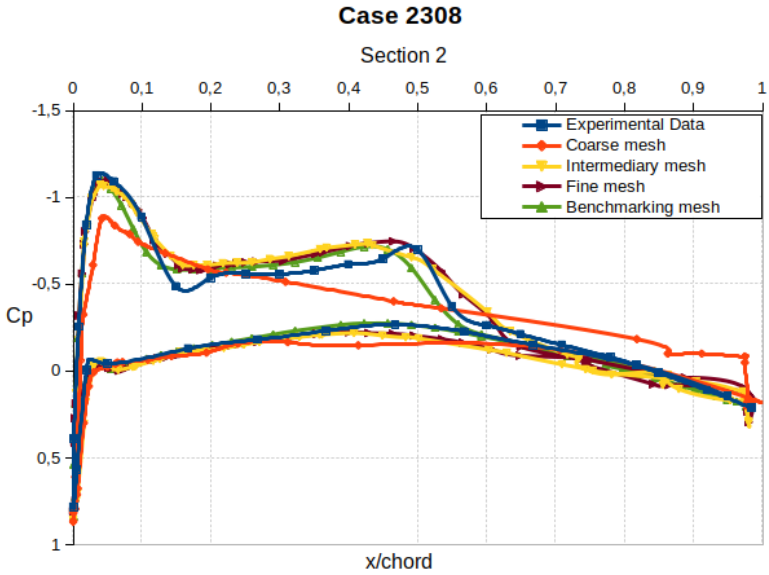

(a) Results of case 2308 for section 2.

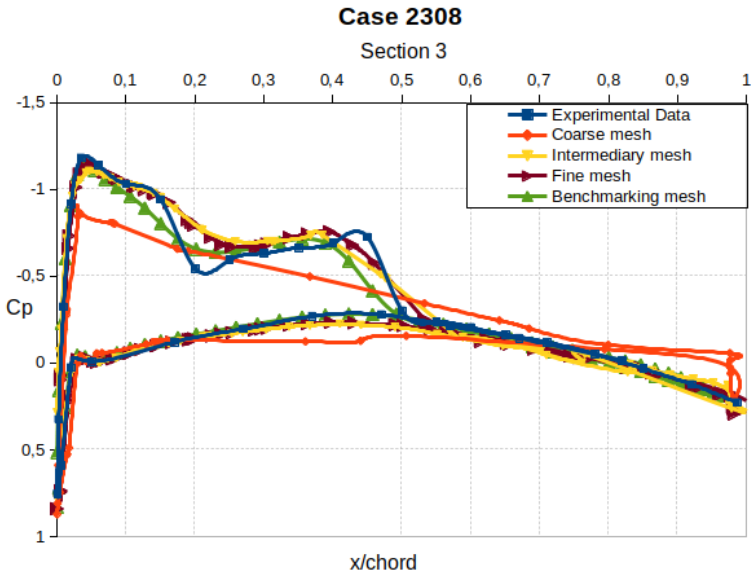

(b) Results of case 2308 for section 3.

Figure 3: Results obtained during the analysis of case 2308 using the SA turbulence model.

Table 4: GCI analysis for case 2308.

Refinement factor r_{21}	$1,3712$
Refinement factor r_{32}	$1,6205$
Approximate relative error e_{a21}	$4,3\%$
Approximate relative error e_{a32}	$7,6\%$
Extrapolated relative error e_{ex21}	$0,9\%$
Extrapolated relative error e_{ex32}	$5,1\%$
Convergence index GCI_{21}	$1,10\%$
Convergence index GCI_{32}	$6,75\%$

Table 4 presents a GCI of $1,10\%$ between the fine and the intermediary mesh and $6,75\%$ between the intermediary and coarse mesh. In this case, for the numerical analysis, must be used the fine mesh.

Decided the mesh, the next step in the study was the test different turbulence models for transonic flows. Besides the SA model, used for the GGI test, was used the k-ω SST turbulence model to compute the turbulence effects. The results

evaluated were also compared with the ones obtained by assume the flow as inviscid and solving this using the Euler equation. To solve the inviscid flow was used the benchmarking mesh that was provided by SU2, found in Economon (2014a). This mesh was developed to simulate case 2308 and consists of an unstructured mesh with 582752 elements.

Figure 4 presents the comparison between SA and k-ω SST turbulence models, and also between the Navier-Stokes equations (used to solve the flow using SA and k-ω SST turbulence models) and Euler equations for the studied case.

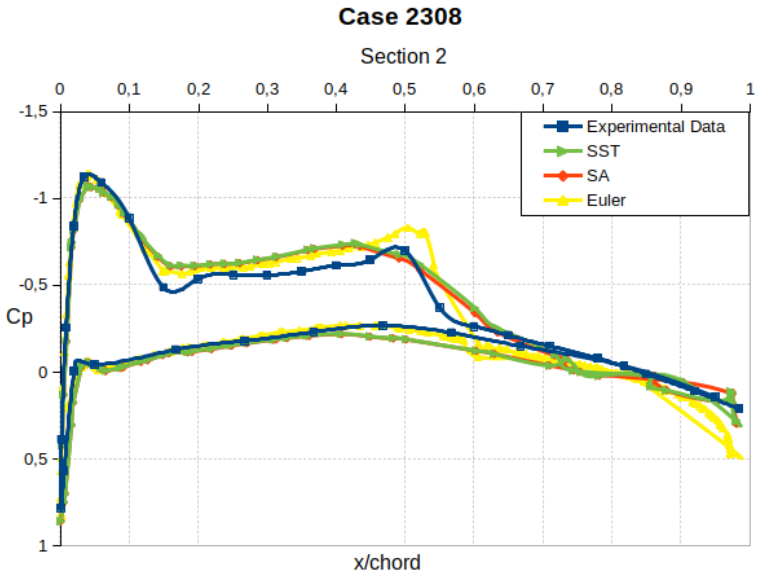

(a) Results of model test for section 2.

(b) Results of turbulence model test for section 3.

Figure 4: Results obtained during the analysis of case 2308 testing turbulence model.

Figure 4 shows that the difference found comparing the results of the Navier-stokes equation (represented by SA and k-ω SST turbulence models curves) with the Euler equations was mainly observed in section 2, where the Cp peak over the upper surface was poorly captured by modeling the fluid flows with the Euler equations. Also, the Euler equation wasn't capable of capture the behavior of the experimental data next to the trailing edge, where de Cp in both sections is greater than the Cp provided by the experimental data, as can be seen in Figure 4, even considering that for the Euler equations solution, was used a benchmarking mesh.

Also, Figure 4 presents that the results evaluated for SA and k-ω SST turbulence models where close. However, the SA model represents a little bit better the behavior of the flow around 0,2-0,3 and 0,4-0,5 of x/c for section 3 of the wing. For this reason, was used the SA turbulent model to solve cases 2306 and 2309.

4.2 Case 2306 analysis

Then, the fine mesh developed for the study (Table 3 presents details about the mesh), and the SA turbulence model were used to simulate case 2306. Figure 5 presents the results evaluated during the analysis.

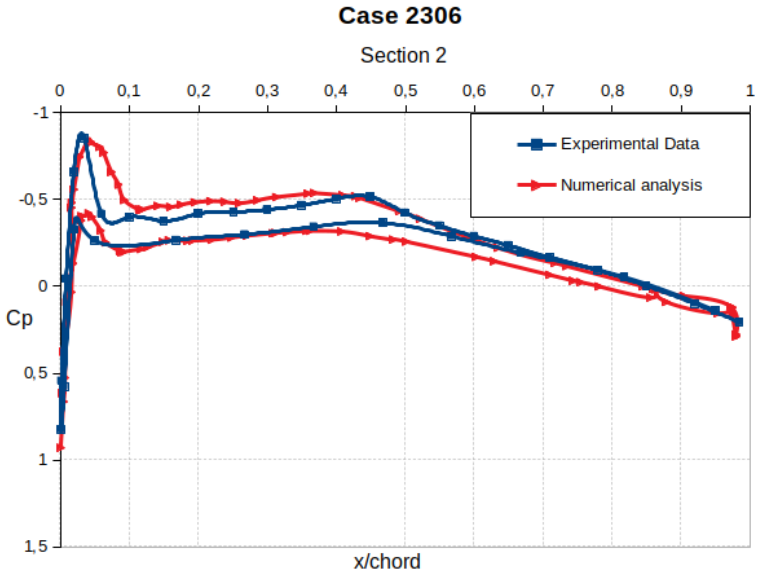

(a) Results of case 2306 for section 2.

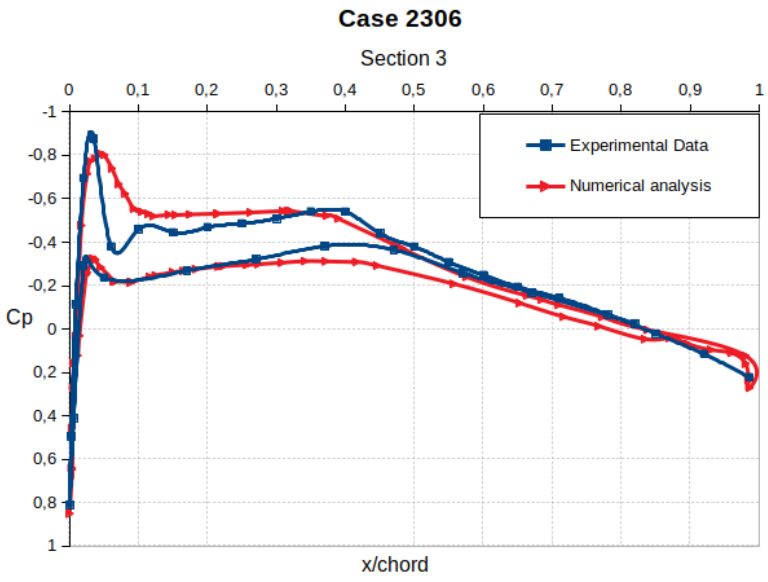

(b) Results of case 2306 for section 3.

Figure 5: Results obtained during the analysis of case 2306.

As can be seen in Figure 5 for case 2306, the numerical data almost fit with the experimental data for the upper surface util 0,2 of x/c, after that the numerical results diverge in value from the experimental data, besides the same behavior is presented by the numerical results curve and the experimental data curve. For the lower surface, however, the numerical results diverge until 0,3 of x/c, after that the numerical results almost fit with the experimental data until 0,8 of x/c, were due to the bad quality mesh generated in the trailing edge the numerical results diverge again from the experimental data.

The divergence between the numerical analysis and the experimental data was due to the mesh. Since Ansys Mesh generates unstructured Tetra/Prism meshes, and this kind of mesh presents poor quality, to solve the problem found in case 2306 is necessary to use another mesh generator.

4.3 Case 2309 analysis

For case 2309, was kept the mesh and turbulence model used in case 2306 simulation. Figure 6 presents the results for the case 2309.

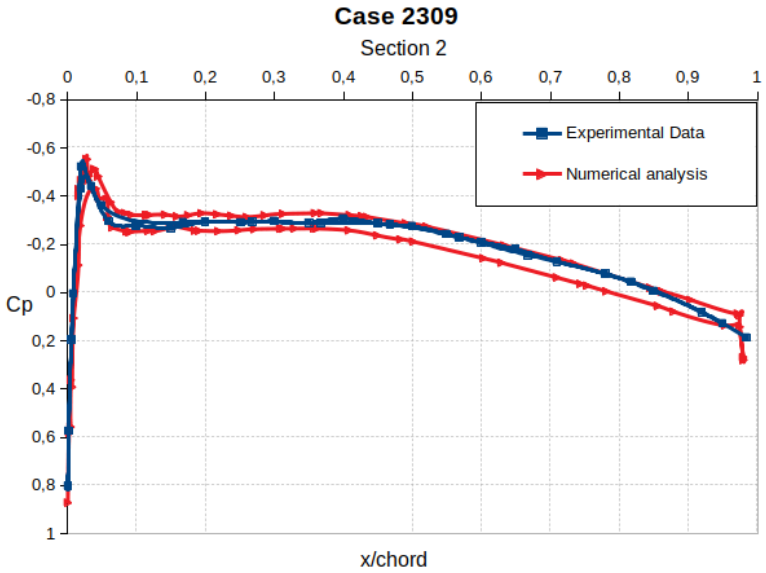

(a) Results of case 2308 for section 2.

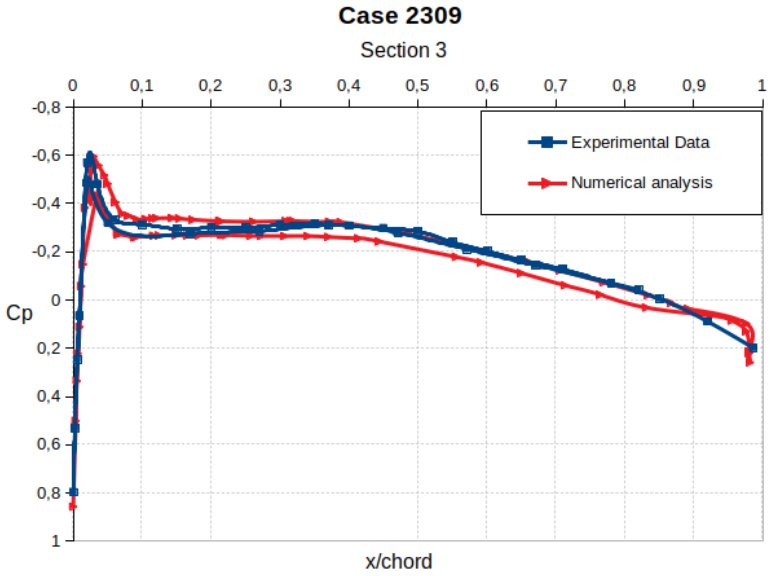

(b) Results of case 2308 for section 3.

Figure 6: Results obtained during the analysis of case 2308.

As can be seen in Figure 6 for case 2309, the numerical data almost fit with the experimental data for the upper surface, only diverging in the trailing edge, what happens due to the poor quality elements generated in the region of the mesh. For the lower surface of the wing, however, the numerical data and experimental data only fit only in the interval of 0 utils 0,4 of x/c. After that, besides keeping the same behavior, the curves evaluated in numerical analysis diverge in value of the curves presented by the experimental data. This problem can be seen in both sections but is more evident in section 3 of the wing.

Besides that, section 3 also presents more errors in representing the behavior of the flow in the trailing edge.

5. CONCLUSIONS

The study concluded that SU2 is capable of solving transonic flow problems, evaluating results with great accuracy, what is seen due to in all the analyzed test cases, the results of the numerical analysis almost fit with the experimental

data.

By the comparison between the SA and the k-ω SST turbulence models was concluded that both models were adequate to represent the flow and solve the closure problem found. The SA turbulence model was preferred due to it represents the behavior of the flow around 0,2-0,3 and 0,4-0,5 of x/c for section 3 of the case 2308 better than k-ω SST.

Comparing the results of the Euler equation with the Navier-Stokes equations results, Figure 4 shows that the Euler equation wasn't capable of capturing the Cp peak over the upper surface, Euler equation also diverges from experimental data next to the trailing.

The major problem found during the study was the mesh generation for SU2 since the software allows just a few mesh types.

Although the native mesh format for the software is the .su2 format, for the study was used .cgns mesh format, this was necessary because just a few mesh generators can generate .su2 meshes, and the authors had access to none of these.

For the analysis, Ansys Mesh was used due to this was the only mesh generator that the authors found that was capable of generating .cgns meshes that provide good results with SU2. Also, it was noticed that for case 2306, the unstructured Tetra/Prism mesh generated by the software didn't present good accuracy as the other test cases presented.

For future studies, the authors pretend to use SU2 to solve more complex transonic flows. The idea is to solve the test cases proposed by AePW-2 (2016) using the BSCW wing geometry.

Another option for future studies is to simulate the flows proposed by this study but changing the mesh generator to observe if the differences found in the analysis, especially for case 2306, can be solved. One possibility is to generate the meshes by using a .su2 mesh generator like Pointwise, Pointwise (2020) presents more information about the software.

6. ACKNOWLEDGEMENTS

This research was supported by resources supplied by the Center for Scientific Computing (NCC/GridUNESP) of the São Paulo State University (UNESP).

7. REFERENCES

AePW-1, 2015. "Aepw-1 homepage". URL <https://c3.nasa.gov/dashlink/static/media/other/AEPW.htm>.

AePW-2, 2016. "Aepw-2 homepage". URL <https://nescacademy.nasa.gov/workshops/AePW2/public>.

Ansys, 2020. "Ansys fluent". <https://www.ansys.com/products/fluids/ansys-fluent>.

ATS, 2020. "Cfd++ homepage". URL <https://www.ats4i.com.br/software/cfd++>.

Begnini, G.R., Spode, C., Pantaleão, A.V., Neto, B.G., Marcório, G.O., Pedras, M.H.J. and Bones, C.A., 2016. "A comparison of cfd and aic-based methods for unsteady aerodynamics and flutter computations of the aepw-2 wing model". *AIAA Aviation*, Vol. 34, No. 3123.

Celik, I., Ghia, U., Roache, P., Freitas, C., Coleman, H. and Raad, P., 2008. "Procedure for estimation and reporting of uncertainty due to discretization in cfd applications". *Journal of Fluids Engineering*, Vol. 130.

CMSoft, 2020. "Aero suite". URL <https://cmsoftinc.com/pages/CMS-AeroSuite>.

Economon, T.D., 2014a. "Inviscid onera m6". <https://su2code.github.io/tutorials/Inviscid_ONERAM6/>.

Economon, T.D., 2014b. "Onera m6 wing". <https://su2code.github.io/tutorials/Turbulent_ONERAM6/>.

Moukalled, F., Darwish, M. and Mangani, L., 2016. *Fluid Mechanics and Its Applications*. Springer International Publishing.

Pointwise, 2020. "Pointwise homepage". URL <https://www.pointwise.com/>.

Raveh, D.E., Yossef, Y.M. and Levy, Y., 2018. "Analyses for the second aeroelastic prediction workshop using the eznss code". *AIAA Journal*, Vol. 56, No. 1, pp. 387–402.

Rumsey, C., 2018. "The spalart-allmaras turbulence model". Technical report, NASA.

Rumsey, C., 2020. "The menter shear stress transport turbulence model". Technical report, NASA.

Sanchez, R., Kline, H.L., Thomas, D., Variyar, A., M., R., Economon, T.D., Alonso, J.J., Palacios, R., Dimitriadis, G. and Terrapon, V., 2016. "Spacecraft thermal control, design, and operation". In *VII European Congress on Computational Methods in Applied Sciences and Engineering*. AIAA.

Schimitt, V. and Charpin, F., 1979. "Pressure distributions onme onera-m6-wig at transonic mach numbers". Technical report, AGARD.

Slater, J.W., 2015. "Onera m6 wing". <https://www.grc.nasa.gov/WWW/wind/valid/m6wing/m6wing.html>.

SU2 Foundation, 2020. "Su2 official website". URL https://su2code.github.io/.

8. RESPONSIBILITY NOTICE

The authors are solely responsible for the printed material included in this paper.